Received: 17 July 2022 | Revised: 8 November 2022 | Accepted: 12 November 2022

DOI: 10.1002/bit.28288

ARTICLE

BIOTECHNOLOGY AND BIOENGINEERING WILEY

Real-time in-situ electrochemical monitoring of *Pseudomonas aeruginosa* biofilms grown on air–liquid interface and its antibiotic susceptibility using a novel dual-chamber microfluidic device

Ye Zhang[1,2] | Hanieh Gholizadeh[2,3] | Paul Young[2,4] | Daniela Traini[2,3] | Ming Li[1] | Hui Xin Ong[2,3] | Shaokoon Cheng[1]

[1]School of Engineering, Faculty of Science and Engineering, Macquarie University, Sydney, New South Wales, Australia

[2]Woolcock Institute of Medical Research, Sydney, New South Wales, Australia

[3]Macquarie Medical School, Faculty of Medicine, Health and Human Sciences, Macquarie University, Sydney, New South Wales, Australia

[4]Department of Marketing, Macquarie Business School, Macquarie University, Sydney, New South Wales, Australia

Correspondence

Shaokoon Cheng, School of Mechanical Engineering, Macquarie University, 44 Waterloo Rd., Macquarie Park, Sydney, NSW 2113, Australia.
Email: shaokoon.cheng@mq.edu.au

Hui Xin Ong, Macquarie Medical School, Faculty of Medicine, Health and Human Sciences, Macquarie University, Sydney, NSW 2113, Australia.
Email: huixin.ong@mq.edu.au

Funding information

Marie Bashir Institute, University of Sydney; Macquarie University Research Excellence Scholarship

Abstract

Biofilms are communities of bacterial cells encased in a self-produced polymeric matrix that exhibit high tolerance toward environmental stress. Despite the plethora of research on biofilms, most *P. aeruginosa* biofilm models are cultured on a solid–liquid interface, and the longitudinal growth characteristics of *P. aeruginosa* biofilm are unclear. This study demonstrates the real-time and noninvasive monitoring of biofilm growth using a novel dual-chamber microfluidic device integrated with electrochemical detection capabilities to monitor pyocyanin (PYO). The growth of *P. aeruginosa* biofilms on the air–liquid interface (ALI) was monitored over 48 h, and its antibiotic susceptibility to 6 h exposure of 50, 400, and 1600 µg/ml of ciprofloxacin solutions was analyzed. The biofilm was treated directly on its surface and indirectly from the substratum by delivering the CIP solution to the top or bottom chamber of the microfluidic device. Results showed that *P. aeruginosa* biofilm developed on ALI produces PYO continuously, with the PYO production rate varying longitudinally and peak production observed between 24 and 30 h. In addition, this current study shows that the amount of PYO produced by the ALI biofilm is proportional to its viable cell numbers, which has not been previously demonstrated. Biofilm treated with ciprofloxacin solution above 400 µg/ml showed significant PYO reduction, with biofilms being killed more effectively when treatment was applied to their surfaces. The electrochemical measurement results have been verified with colony-forming unit count results, and the strong correlation between the PYO electrical signal and the viable cell number highlights the usefulness of this approach for fast and low-cost ALI biofilm study and antimicrobial tests.

KEYWORDS

air–liquid interface, antibiotic susceptibility, biofilm growth, dual-chamber microfluidic device, electrochemical monitoring

1 | INTRODUCTION

Bacteria play crucial roles in the ecological system. While they are generally notorious for threatening human health and causing significant losses in industries, their existence can be beneficial, such as balancing gut health, purifying wastewater, maintaining soil moisture, and so forth. It has been well-recognized that most bacteria live in a community model known as biofilms instead of acting alone as planktonic cells. Biofilm formation commences when planktonic bacteria adhere to a surface and form irreversible attachments. The anchored bacteria multiply and produce an extracellular polymeric substance (EPS), gradually forming a complex three-dimensional (3D) biofilm structure that matures over time, which ensues infectious bacteria's dispersal to colonize other areas (Ranganathan, 2014). Biofilm maturation promotes bacteria's communication and enhances their tolerance against adverse conditions, thus improving survival. In medical microbiology, biofilms are typically involved in chronic persistent infections (Bjarnsholt, 2013). For example, many chronic lung infections, such as cystic fibrosis, chronic obstructive pulmonary disease, and bronchiectasis, are caused by persistent *Pseudomonas aeruginosa* biofilms developed in the respiratory tract system (Jamal et al., 2018; Maurice et al., 2018). *P. aeruginosa* is a pathogen that could establish a biofilm within 24 h and progress to infection rapidly (Park et al., 2011). Ciprofloxacin (CIP) is a broad-spectrum antibiotic effective against *P. aeruginosa* (Brazas & Hancock, 2005).

Several *in vitro* models have been developed to study the properties of biofilm and evaluate the efficacy of biofilm control approaches. Some of these models include the microtiter plate (Peeters, et al., 2008), the Center for Disease Control biofilm reactor (Williams & Bloebaum, 2010), the rotating disk biofilm reactor (Schwartz, et al., 2010), the Calgary Biofilm Device (Ceri et al., 1999), and microfluidic devices (Kim et al., 2010). However, most of these models are only limited to the culturing of biofilm on the solid–liquid interface (SLI) despite biofilm being capable of developing on diverse interfaces such as air–liquid interface (ALI), liquid–liquid interface (LLI), and solid–air interface. The interface could affect critical aspects that undermine biofilm proliferation, such as attachment, nutrient uptake, and mass exchange. At least one study has demonstrated that biofilm susceptibility to treatment likely differs depending on whether they proliferate on ALI or LLI. Permeability of the biofilms, for example, has been demonstrated to be different between biofilms developed on ALI and LLI (Zhang, Silva, Young, et al., 2022). Hence, selecting a suitable interface to develop efficient biofilm-killing approaches is crucial. For example, the biofilm formation in the respiratory tract system should be modeled as ALI biofilm to reveal more accurate information for biofilm-caused infections.

Several methods have been used to study biofilm's growth profiles and viability (Azeredo et al., 2017). The colony-forming unit (CFU), for example, has been used to determine the viable cell numbers within biofilm samples (Emanuel & Lorrence, 2021). However, analyzing the CFU is an end-point measurement and requires sacrificing the biofilm sample. This method of assessing biofilm's viability is also time-consuming and requires large amounts of reagents and consumables. Biofilm viability *in-situ* has also been analyzed based on the presence of fluorescent proteins. However, these methods must use genetically modified bacteria of selective labels and requires expensive optical equipment.

Electrochemical monitoring is a sensitive technique that can be used to detect biological substances in real-time (Sezgintürk, 2020), and these sensors can be broadly classified into two different types, namely impedimetric/nonfaradaic and faradaic (potentiometric, amperometric) transducers (Subramanian et al., 2020). Electrochemical detection of biofilm growth relies on the fact that bacterial biofilm produces many molecules that promote communication and defend the colony (Lau et al., 2004; Miller & Bassler, 2001; Willcox et al., 2008). These molecules can undergo reversible redox (exchange of electrons) reactions, which can be detected by electrochemical methods. For example, *P. aeruginosa* species specifically produces the blue electro-active molecule pyocyanin (PYO), which is a useful marker of cell viability and virulence (Lau et al., 2004; Willcox et al., 2008; Žukovskaja et al., 2017). Existing work has demonstrated that the concentration of PYO in the lung of cystic fibrosis patients is very high (up to 100 μM) (Caldwell et al., 2009). PYO can be measured by square wave voltammetry (SWV) over the range of voltages where it is reduced by the following reaction: $[PYO]_{OX} + 2H^+ + 2e^- \leftrightarrow [PYO]_{red}$ (Webster & Goluch, 2012).

New advances in real-time *in-situ* electrochemical monitoring of biofilm have been introduced in recent years, and many of them are related to improving the sensitivity of this technique (Bai et al., 2018; Erbay, 2016; Song et al., 2020). For example, new carbon nanomaterial (e.g., carbon nano pods, carbon nanotubes, and graphene) for the sensors has been introduced, along with the different approaches to realize low-cost electrochemical sensors (Subramanian et al., 2020). Other improvements in this area include the design of microfluidic devices. Microfluidic devices have been commonly used as bacteria cell culture platforms (Pérez-Rodríguez et al., 2022) due to their simplicity for fabrication, low consumption of reagents, and excellent control of experimental conditions. In contrast, real-time biofilm sensing, characterization, and evaluating treatment using microfluidic devices remain rare. Webster et al. (2015) used a disposable three-electrode cell (Zensor TE100) in a microfluidic chamber and studied the killing of *P. aeruginosa* biofilm using different concentrations of antibiotic solution. In the study, the biofilms were cultured on the SLI model, and information on the real-time growth of *P. aeruginosa* biofilm on ALI remains scarce.

This study aims to investigate the growth characteristics of *P. aeruginosa* biofilm developed on ALI and its antibiotic susceptibility using the electrochemical detection method. A dual-chamber microfluidic device integrated with three electrodes, using Conical carbon nanofibers (CNFs) modified carbon electrode, Ag/AgCl wire and platinum (Pt) wire as working electrode (WE), reference electrode (RE), and counter electrode (CE), respectively, were designed and developed. The dual-chamber device was designed to enable biofilm to be cultured on the ALI and allows the antibiotic solution to be

delivered to the biofilm via the top or bottom chamber of the microfluidic device. Since PYO is a marker for *P. aeruginosa*'s viability, we hypothesized that the amount of PYO produced by bacterial cells in the ALI biofilm is correlated with its viable cell number, and the production rate may vary during its growth depending on the number of bacteria that compete for the limited nutrient resource. Furthermore, we hypothesized that the antimicrobial effect of CIP solution is concentration-related and different drug delivery approaches may have different biofilm-killing outcomes.

2 | EXPERIMENTAL

2.1 | Device fabrication

Figure 1a illustrates the schematics of the dual-chamber microfluidic design integrated with electrodes. The device consists of two layers of polydimethylsiloxane (PDMS) films which form the top and bottom chamber. There are two 3D-printed covers, one of which is embedded with three electrodes. A porous membrane (Polyester, hydrophilic, 0.2 µm, Sterlitech) is sandwiched between the top and bottom chambers and serves as the substratum for bacteria attachment and biofilm development.

The 3D-printed covers and the moulds for casting the PDMS film were designed using Creo software (PTC) and printed using the clear resin on a Form2 stereolithographic 3D printer (Formlab Inc.). Freshly printed parts were washed with isopropyl alcohol for 15 min and then post-cured with ultraviolet radiation at 65°C for 1 h using the Form Wash and Form Cure finishing stations (Formlab Inc.), respectively. The three electrodes were embedded in the top cover, with three groves with the dimensions of 1.5 mm × 0.5 mm, 0.4 mm × 0.4 mm, and 0.6 mm × 0.6 mm, for pasting carbon electrodes and placing Ag/AgCl wire and Pt wires, respectively.

Carbon conductive cement (CCC; Electron Microscopy Sciences) was used as a solvent-resistant adhesive to prepare the carbon electrode. CNFs (Sigma Aldrich) were added to the CCC to modify the electrical conductivity of the WE. To prepare the CNFs-modified carbon (CNFs-C) electrodes, CNFs were dispersed in the CCC thinner (6 mg/100 µl) agent by sonication for 5 min. Next, the suspension was mixed with the CCC manually until a paste with a uniform texture was obtained. The paste was then applied to the 3D-printed cover, compressed, spread homogeneously using a spatula, and dried for 30 min at room temperature.

The top and bottom chambers were fabricated using PDMS by 3D printing microfluidic fabrication technique (Amin et al., 2016). The 3D-printed and UV-cured mould was spray-coated with Ambersil PUR 400 release agent (CRC Industries UK Ltd., Corning) before pouring the PDMS into it to protect the mould surface and assist with the PDMS removal after the curing process. The PDMS base and curing agent (Sylgard 184; Dow Corning) were mixed at 10:1 w/w and degassed using a vacuum desiccator chamber before and after being transferred into the moulds and subsequently cured at 65°C for 3 h. The dimension of the chamber is 6 mm (length) × 1 mm (width) × 1 mm (height).

2.2 | Device assembly

The assembled device is shown in Figure 1b. Reversible mechanical bonding of the multiple layers was achieved by four screws and nuts positioned around the perimeter of the flow chamber to secure the alignment of the layers and interfaces between the two chambers. The Pt wire (99.9% purity, 250 µm diameters; Sigma Aldrich) and the sintered Ag/AgCl wire (203 µm diameters; A-M System) were embedded into the grooves on the top cover.

22 G blunt needles (Livingstone) closed with a plastic cap were inserted into the inlets of the chambers, and 22 G stainless-steel couplers (Livingstone) connected with Tygon tubing (1.59 mm OD x 0.51 mm ID; Darwin Microfluidics) were inserted to the outlets of the chambers. The other end of the Tygon tubing was connected to

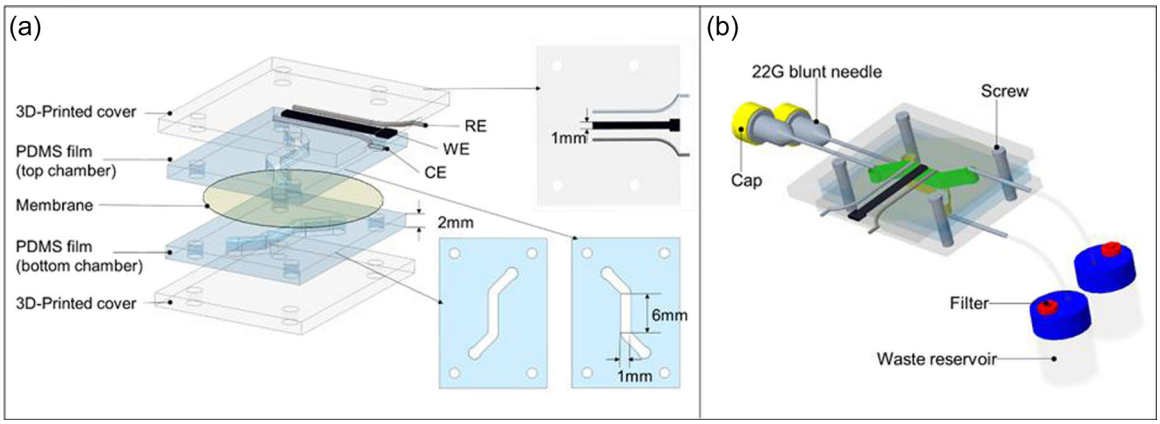

FIGURE 1 (a) The construction of three electrodes integrated dual-chamber microfluidic design. (b) The assembled device for biofilm culture and electrochemical detection. PDMS, polydimethylsiloxane.

the waste reservoirs via fittings (IDEX). A 0.4 µm sterile filter (0.4 µm PTFE, 25 mm; Simplepure) was connected to each waste reservoir to maintain the bottle's atmospheric pressure and ascertain a sterilized environment. Epoxy glue was applied to prevent any opening around the needles and electrodes in the assembled devices.

2.3 | Electrochemical performance of the dual-chamber microdevice

Electrochemical PYO detection was performed using CNFs-C, Pt, and Ag/AgCl electrodes as the WE, CE, and RE. Phosphate-buffered saline (PBS, Sigma Aldrich) was used as the supporting electrolyte for electrochemical analysis by the CNFs-C electrode.

2.3.1 | Optimization of the CNFs-C electrode composition

To optimize the electrochemical performance of the CNFs-C electrode for PYO detection, the CNFs content was varied by mixing CNFs and CCC at different mixing ratios (mg/mg): 0 (CCC only), 6:100, 12:100, 18:100, and 24:100, and the obtained response currents were evaluated. SWV was performed to analyze the electrochemical performance of the electrode. SWV was chosen due to its sensitivity in detecting the electrochemical peak of PYO compared with other voltammetric and amperometric techniques (Webster et al., 2015). The voltammograms were obtained for 10 µM PYO (Sigma Aldrich) solution in PBS and the blank (supporting electrolyte, PBS) solution. Approximately 100 µl solution was injected into the top chamber. The potential was scanned using a PGSTA204 potentiostat (Metrohm Autolab) following a staircase function combined with a small potential pulse at each step. SWV was performed within −0.5 to 0.2 V potential range with 5 mV step potential, 50 mV modulation amplitude, 15 Hz frequencies, and at a 0.067 s time interval. The increase in the peak current (peak height; I_{pa}) such that it becomes more distinct and apparent with modified electrodes was investigated. Two devices were assembled with each composition, and each device was scanned three times. The CNFs-C electrode with optimized composition was then used for further experiments.

2.3.2 | Electrochemical quantification of PYO by CNF-C electrode

The CNFs-C electrode was calibrated to be used for PYO quantification. SWV described in Section 2.3.1 was performed for solutions with varying PYO concentrations ranging from 1 to 100 µM. The PYO oxidation peak current values (I_{pa}) were then plotted against the PYO concentration (C_{PYO}), and this information was subsequently used to quantify PYO excreted by the ALI *P. aeruginosa* biofilm in the study. Two dual-chamber microfluidic devices integrated with optimized CNFs-C electrodes were used for the test. The dilution series was repeated twice, and each concentration was measured in triplicates.

2.4 | Device inoculation and biofilm culture

Before inoculation, all the components were assembled aseptically in the biosafety cabinet and sterilized using the autoclave (121°C/20 min). *P. aeruginosa* (PAO1, ATCC 15692, American Type Culture Collection [ATCC]) from frozen stocks were grown on agar plates for 16–18 h at 37°C. The liquid preculture was prepared by transferring one *P. aeruginosa* colony into 1 ml of Cation-adjusted Mueller–Hinton Broth (CaMHB; BD Biosciences), incubated for 16–18 h at 37°C, and shaken at 200 rotations per minute (RPM). The overnight preculture was diluted at 1:30 v/v in fresh media, incubated for 2 h at 37°C, and shaken at 200 RPM to make an inoculum with OD_{600} = 0.4 (Zhang, Silva, Traini, et al., 2022). The consistency of the inoculum size was verified by viable CFU counts. After removing the caps of inlet syringe needles, approximately 100 µl inoculum and 100 µl CaMHB media were loaded into the top chamber and bottom chamber, respectively, at a flow rate of 100 µl/min using the syringe pump (Chemyx Fusion 200; Chemyx Inc.). After loading the bacteria and media, the inlets were closed with caps, and the device was placed in the incubator at 37°C for 2 h to allow planktonic bacteria to attach to the membrane.

After bacteria attachment, the inoculum in the top chamber was replaced by the air injected from the top chamber inlet at a flow rate of 100 µl/min for 5 s. Subsequently, the ALI was created for biofilm growth, and the device was placed in the incubator at 37°C for biofilm formation for 48 h.

2.5 | Antibiotic treatment

To assess the susceptibility of the ALI biofilm to CIP solution and investigate the efficacy of the two different drug delivery routes (top chamber exposure and bottom chamber exposure, respectively), after 48 h growth on ALI, the culture media in the bottom chamber was flushed from the chamber, followed by injecting approximately 100 µl antibiotic solution into the top chamber or the bottom chamber at a flow rate of 100 µl/ml. A stock solution of CIP was prepared in PBS, and working solutions 50, 400, and 1600 µg/ml were freshly prepared by diluting the stock in PBS. The antibiotic concentration range was selected based on our previously published study (Zhang, Silva, Traini, et al., 2022), which covers the minimum biofilm eradication concentration (MBEC) of CIP solution for treating 48-h old ALI biofilm cultured using the dual-chamber microfluidic device under the static condition. The control group was treated with PBS solution (0 µg/ml). After the solution was injected into the chamber, the device was placed in the incubator at 37°C for 6 h. The electrochemical measurement of PYO and CFU counts was conducted after 6 h exposure.

2.6 | Electrochemical monitoring

Electrochemical measurements of PYO were performed at different time points (6, 24, 30, and 48 h) during biofilm growth and after 6 h antibiotic treatment. The SWV method described in Section 2.3.1 was applied to perform the measurements. Before bacteria inoculation, the top chamber was loaded with PBS solution, and the measurement was performed as blank control. After 2 h, the ALI was established for biofilm growth, and the SWV measurement was conducted at 6, 24, 30, and 48 h. At the time of measurement (Figure 2), the culture media in the bottom chamber was pushed out of the chamber using a syringe and approximately 100 µl PBS solution was injected into the top chamber at a flow rate of 100 µl/min. After the top chamber was filled with PBS solution, the device was turned upside-down and kept stationary for 15 min in the incubator at 37°C before PYO quantification by SWV. After the SWV measurement, the PBS solution in the top chamber was pushed out from the top chamber at a flow rate of 100 µl/min, and approximately 100 µl CaMHB media was filled into the bottom chamber. Subsequently, the same device was continuously monitored and was treated the same way before SWV measurement. The electrochemical monitoring of ALI biofilm growth was repeated with 36 samples (6 technical replicates × 6 biological replicates).

For the detection of PYO after 6 h of antibiotic solution exposures, the bottom chamber was emptied using a syringe and approximately 100 µl of PBS solution was injected into the top chamber at a flow rate of 100 µl/min, and the PYO concentration was measured after the dual-chamber device was turned upside-down and kept still for 15 min in the incubator at 37°C. The test was repeated six times (3 technical replicates × 2 biological replicates) for each antibiotic solution concentration.

2.7 | Biofilm viable cell number count

The production of PYO is correlated with the number of viable *P. aeruginosa* cells within the biofilm. Thus, the viable bacteria cell number within the biofilm after 6, 24, 30, and 48 h of growth, followed by 6 h of antibiotic exposure was analyzed using CFU count (Zhang, Silva, Traini, et al., 2022). At the time of sample collection, the membranes with the biofilm samples were picked up from the device, rinsed with 1 ml sterile PBS, and then transferred to a tube containing 1 ml of sterile PBS for 280 s sonication at 47 kHz and 1.8 W/cm^2 to dissolve biofilm bacteria in solutions. Ten-fold serial dilutions of the PBS sonicated bacteria suspensions were performed in sterile PBS, plated on LB agar (Sigma Aldrich) plates, and incubated at 37°C for 16–18 h. Viable colony counts were calculated using the following equation:

$$\mathrm{CFU/ml} = \frac{N \times 10}{10^{-D}}, \quad (1)$$

where N represents the colony number and D represents the number of 1:10 dilutions. The biofilm viability experiments were repeated three times using different batches of inoculum, and three samples were collected in each batch. The test for each condition was repeated six times (3 technical replicates × 2 biological replicates). The rationale for the calculation method is that the analysis of the viable biofilm cell number can be consistent with a previous work (Zhang, Silva, Traini, et al., 2022) to provide a meaningful comparison between ALI biofilms cultured under different environmental conditions.

2.8 | Statistical analysis

Unless otherwise stated, the experiments were performed in six replicate. Data are expressed as mean ± standard error of the mean and significance of difference between mean values was determined by unpaired *t*-test or one-way analysis of variance (ANOVA) for two or three groups of data, respectively. Data sets with a $p < 0.05$ were considered as significantly different. All the statistical analysis was performed using GraphPad Prism 7.0.

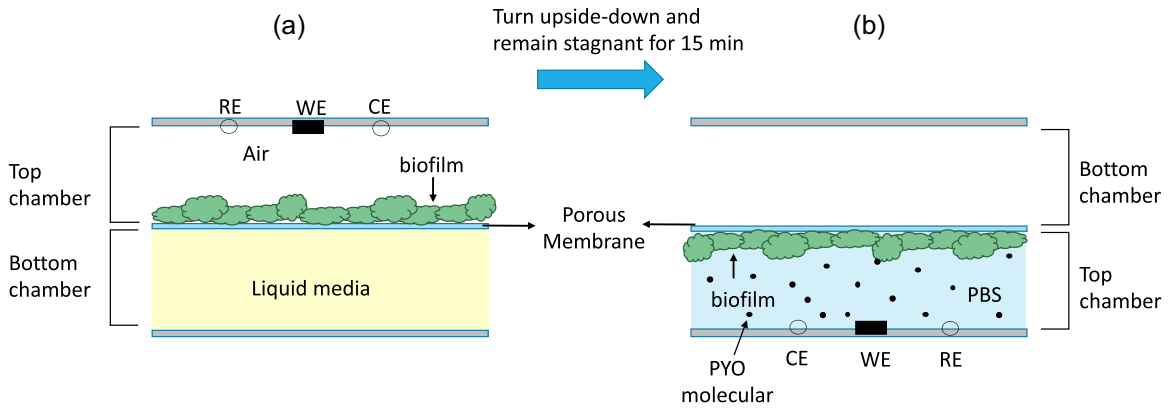

FIGURE 2 (a) Illustration of biofilm developed on ALI using three electrodes integrated dual-chamber microfluidic device. (b) Illustration of the PYO detection of ALI biofilm using three electrodes integrated dual-chamber microfluidic device. ALI, air–liquid interface; CE, counter electrode; PBS, phosphate-buffered saline; PYO, pyocyanin; RE, reference electrode; WE, working electrode.

3 | RESULTS AND DISCUSSION

3.1 | Optimization of the CNFs-C electrode composition for PYO detection

The effects of the electrode composition on the PYO oxidation peak current were determined using WEs prepared with five CNFs: CCC (w/w %) percentages, 0%, 6%, 12%, 18%, and 24%, respectively. Figure 3a shows that the PYO oxidation peak appeared within the range of −0.4 to −0.2 V with all the CNFs-C electrodes. This result corresponds well with the study of the voltammetric behavior of PYO using the commercial available and disposable three electro cell (Zensor TE100) (Webster et al., 2015). This suggests that the electrodes integrated with the dual-chamber microfluidic device can detect PYO and can produce accurate measurements that match with existing work. It has been reported that CNFs modified CCC materials retain their properties very well in aqueous media despite prolonged contact time (Gholizadeh et al., 2021). Moreover, compared with commercial electrodes, the carbon electrode's composition can be modified to improve the sensitivity of the measurement, and the ease of manufacturing the electrodes also enables them to be incorporated in other locations of the device to allow for flexibility in design.

The response oxidation peak currents (I_{pa}) were obtained after baseline correction, with the result shown in Figure 3b. One-way ANOVA was used, and significant differences between the average peak currents of the CNFs modified electrodes and the electrodes made with pure CCC were determined. The statistical analysis shows that when detecting the same concentration of PYO (10 μM), the I_{pa} value obtained by electrodes containing 18% CNFs in the composition is the highest ($I_{pa} = 0.054 \pm 0.024$ μA) and is significantly different ($p < 0.05$) compared to the pure carbon electrode. It shows that the current peak detected by the electrodes made with CCC is the lowest ($I_{pa} = 0.028 \pm 0.014$ μA) compared with other electrodes mixed with CNFs. The I_{pa} value gradually increases with the increase of the CNF ratio until it reaches 18%. This demonstrates that the excellent electrical conductivity of the conical CNF improves the electrochemical performance of the electrodes (Gholizadeh et al., 2021). However, the subsequent addition of CNF in the electrode composition to 24% did not further improve its performance. This could potentially be related to the poor homogeneity of CNFs content on the CCC adhesive, and a high localized concentration of CNF has been demonstrated to negatively affect the electrical properties of the electrodes (Gholizadeh et al., 2021). Therefore, the maximum peak current was observed for the CNF-C electrode with 18% CNFs and this electrode composition was used for all subsequent experiments. It is also observed that the PYO oxidation on the CNFs-C electrode occurs at 0.3 ± 0.05 V potential for all the electrodes tested.

3.2 | Electrochemical quantification of PYO by CNFs-C electrode

The optimized CNFs-C electrode was calibrated to quantify and monitor PYO excretion from biofilms developed under ALI condition in the dual-chamber microfluidic device. Figure 4a presents the square wave voltammograms obtained from the optimised CNFs-C electrode, showing that the PYO oxidation peak consistently appears within the potential range of −0.4 to −0.2 V and the value of peak current I_{pa} increases as the PYO concentration increases. Each concentration's averaged peak current value was calculated ($N = 6$), and the dependence of PYO oxidation peak current on PYO concentration was determined and illustrated in Figure 4b. A linear relationship ($R^2 = 0.998$) between the two parameters (I_{pa} and C_{PYO}) was obtained within 1–100 μM concentration range, which was subsequently used as the calibration reference for the real-time quantification of PYO excretion during the growth of biofilm under ALI condition.

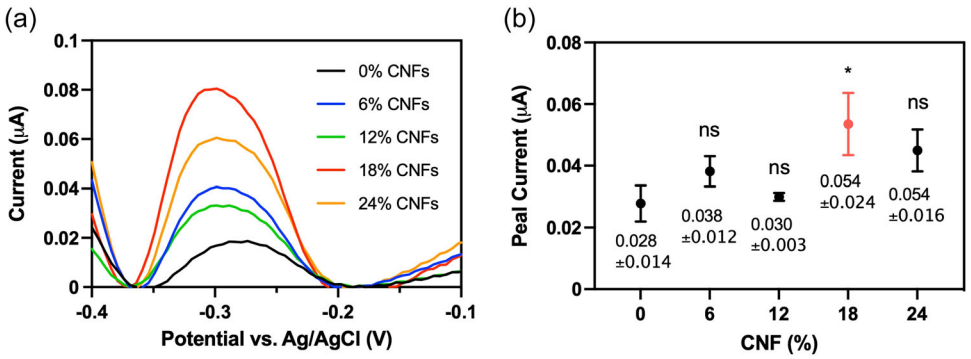

FIGURE 3 Optimisation of the CNFs-modified carbon electrode's electrochemical response for voltammetric PYO detection, where electrodes prepared with different CNFs: CCC (w/w) % were tested for measuring 10 μM PYO in PBS (pH 7). Square wave voltammetry was performed from −0.5 to 0.2 V at a frequency of 15 Hz and an amplitude voltage of 50 mV. (a) Representative voltammograms for each electrode tested; (b) comparison of the oxidation peak currents (I_{pa}) observed in the voltammograms ($N = 6$, mean ± SEM). A significant difference from the electrode with pure CCC (0%) is indicated (*, $p < 0.05$; ns, not significant). CCC, Carbon conductive cement; CNF, carbon nanofiber; PYO, pyocyanin.

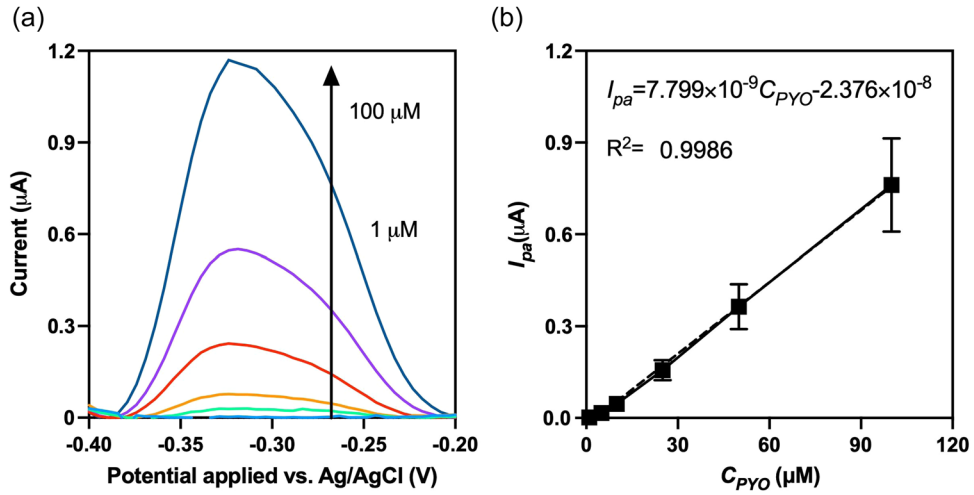

FIGURE 4 (a) Square wave voltammograms of series dilution of PYO in PBS (pH 7) from 1 to 100 μM using the CNFs-modified carbon (18%) electrodes integrated dual-chamber microfluidic device. (b) The analysis of the dependence of PYO oxidation peak current ($N = 6$) to PYO concentration in PBS (pH 7). Square wave voltammetry was performed from −0.5 to 0.2 V at a frequency of 15 Hz and an amplitude voltage of 50 mV. C_{PYO}, concentration; I_{pa}, peak current of PYO in PBS. Error bars represent the standard deviation of the mean for six samples. PBS, phosphate-buffered saline; PYO, pyocyanin.

3.3 | Monitoring the growth of ALI biofilm

Optimizing the design of the microfluidic device such that it has a controlled environment to recapitulate how biofilms strive and develops to maturity in ALI realistically has been reported in the authors' previous study (Zhang, Silva, Traini, et al., 2022), where biofilm samples have been characterized by CFU count, crystal violet staining and microscope imaging. To quantify electro-active PYO molecules produced by *P. aeruginosa* biofilm during growth under ALI condition in the dual-chamber microfluidic device, SWV was conducted at 6, 24, 30, and 48 h postseeding. Figure 5 shows the obtained voltammograms at each time point of the *P. aeruginosa* biofilm growth. The PYO oxidation peak was observed in the obtained voltammograms at all time points of the measurement, suggesting the continuous growth of the bacteria in the device, forming a biofilm under stationary ALI condition and producing PYO during growth. The change in the oxidation potential (where the peak current was measured) is likely related to that the surface potential of the Ag/AgCl RE has varied slightly because of their exposure to the test solution. A similar observation was reported in an existing work where a slight change in the surface potential of Ag/AgCl RE during detection has been demonstrated (Shinwari et al., 2010).

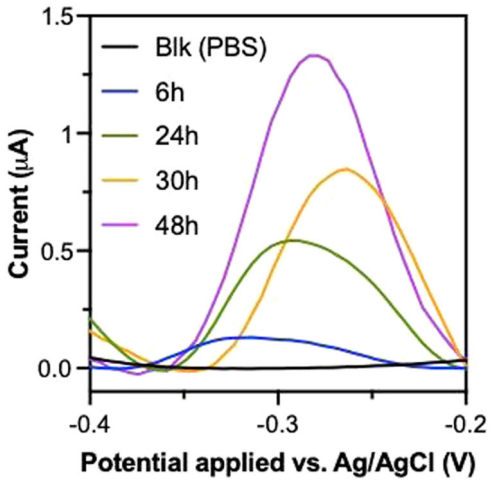

FIGURE 5 Representative SWV scans of pyocyanin produced by PAO1 during culture under air–liquid interface condition in the dual-chamber microfluidic device at 6, 24, 30, and 48 h. SWV scans were performed from −0.5 to 0.2 V at the frequency of 15 Hz and an amplitude voltage of 50 mV. PBS, phosphate-buffered saline; SWV, square wave voltammetry.

The peak current of each measurement was converted to PYO concentration using the linear equation obtained in Figure 4, and the accumulated production of PYO during the growth of ALI biofilm was analyzed and reported in Figure 6a. The data were analyzed using an unpaired *t*-test and compared to the control group (device inoculated with PBS), a significant difference ($p < 0.0001$) was observed across the measurements at all time points. Results show that PYO increased throughout the 48 h growth period. To investigate how the PYO production rate may have changed during the growth period, the averaged PYO production rate (the production of PYO per hour) at different phases of the biofilm growth was calculated, and the result is shown in Figure 6b. One-way ANOVA was used, and significant differences were demonstrated between the averaged PYO production rates during the initial 6 h and all the subsequent growth phases. Results from the current study show that, during the initial 6 h, the PYO production rate was approximately 9 μM/h. As the biofilm proliferated, the PYO production rate increased significantly and reached a maximum value (30 μM/h) between the 24 and 30 h growth phase. However, between the 30 and 48 h growth phase, the production rate reduced to 10 μM/h, and this is not significantly different from the production rate at the initial growth phase (0–6 h). It has been reported that PYO production

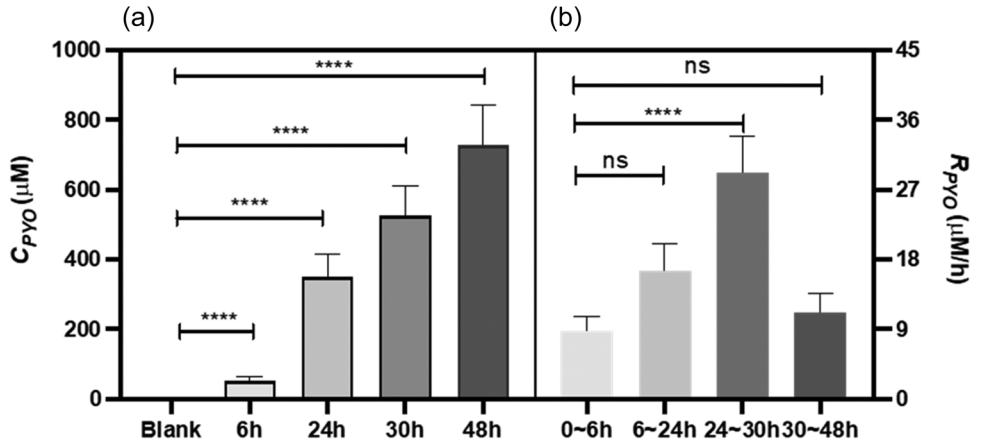

FIGURE 6 (a) The accumulated production of PYO detected by the electrochemical method at various time points. The significant difference compared with the blank control group (unpaired *t*-test) as indicated (****$p < 0.0001$). (b) The production rate of PYO (R_{PYO}) during different growth phases. The significant difference compared to the production rate at the 0–6 h growth phase (one-way ANOVA) as indicated (****$p < 0.0001$; ns, not significant). Error bars represent the one standard deviation of the mean for 36 samples. ANOVA, analysis of variance; PYO, pyocyanin.

is closely related to the biofilm's metabiotic status and viability (Allen et al., 2005). Our results show that biofilm grown under the ALI condition in the microfluidic device constantly produces PYO, and the production rates varied during a 48 h growth period. The exact cause of the variability in the PYO production rate is unclear and could be related to several plausible reasons. For example, biofilm formation starts with planktonic cells attached to the porous membrane when culturing biofilm on ALI using the dual-chamber microfluidic device. The defined amount of culture media in the bottom chamber provides nutrients for the biofilm's development. At the initial stage of biofilm formation, the number of bacteria competing for this limited nutrient resource is relatively low; thus, the biofilm can proliferate much faster, represented by the high PYO production rate during this period. However, as the nutrients deplete over time, the metabolism of the biofilm decreases, with some bacteria potentially becoming dormant (Akiyama et al., 2018; Stoodley et al., 1998), resulting in the reduced PYO production rate as demonstrated through this current work.

Living *P. aeruginosa* cells constantly produce PYO during the formation of biofilm (Lau et al., 2004). To further investigate the relationship between the viable cell number in the biofilm and the production of PYO, samples after 2 h attachment and 6, 24, 30, and 48 h growth were collected. The viable bacteria cell numbers were determined using the CFU count method, and the analyzed results are shown in Figure 7. The CFU number of the various collected samples (see Figure 7a) shows that the older the biofilm, the more viable cells and viable cell numbers it contains. One-way ANOVA was used to compare the CFU number of the biofilm samples with the CFU number of attached cells for initiating biofilm formation. A statistically significant difference was observed after 24 h growth.

To further investigate the cell proliferation rate, the average increase in bacteria per hour during different growth phases was calculated using Equation (2), and the result is shown in Table 1

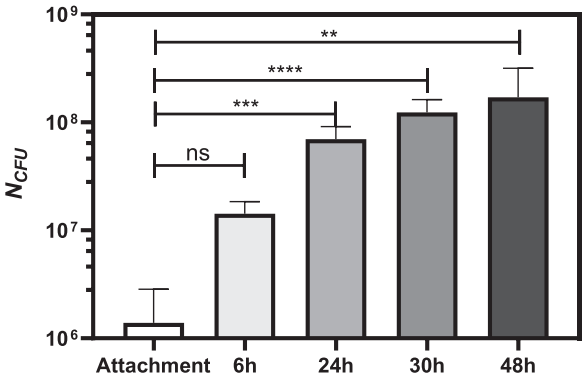

FIGURE 7 The CFU number of various ages of biofilm samples (N_{CFU}). Significant difference compared with the attachment group (one-way ANOVA) is indicated (**$p < 0.01$; ***$p < 0.001$; ****$p < 0.0001$; ns, not significant). Error bars represent the one standard deviation of the mean for the six samples. ANOVA, analysis of variance; CFU, colony-forming unit.

$$\text{Bacteria proliferation rate} = \frac{\text{Averaged } N_{CFU}(i) - \text{Average } N_{CFU}(i-1)}{T(i) - T(i-1)}, \quad (2)$$

where i represents the sample collection time point, and $T(i)$ is the age of the biofilm sample.

The data shows that the biofilm bacteria proliferation rate starts with 3.2×10^6 CFU/h during the initial 6 h growth, and a similar proliferation rate was observed between the 6 and 24 h growth phase. The proliferation rate increased by close to three-fold and reached a maximum value (8.9×10^6 CFU/h) during the 24–30 h growth phase. The proliferation rate slowed and dropped to 2.6×10^6 CFU/h between the 30 and 48 h growth phase. It can be observed that the growth trend of the bacteria proliferation rate aligns with the trend of the PYO production rate, as demonstrated in

TABLE 1 The averaged biofilm bacteria proliferation rate of various growth periods

Growth period	Bacteria proliferation rate (CFU/h)
Attachment −\6 h	3.2×10^6
6–24 h	3.0×10^6
24–30 h	8.9×10^6
30–48 h	2.6×10^6

Abbreviation: CFU, colony-forming unit.

Figure 6b. The above strongly suggests that the production rate of PYO correlates to biofilm bacteria cells' proliferation rate.

To further determine if the production of PYO is proportional to the viable bacteria cell number, a scatter plot (Figure 8) was obtained using the average value of CFU number of biofilm samples collected at different time points and the averaged accumulated PYO concentration determined at the corresponding time point. As shown in Figure 8, a linear trend ($R^2 = 0.9937$) was established, providing evidence on the proportional relationship between the amount of PYO produced by bacterial cells in ALI biofilm and the number of viable cells. In addition, it is usually very challenging for conventional microscale models and techniques to control biofilm development due to their inability to control environmental conditions (Pérez-Rodríguez et al., 2022). Microfluidic devices can provide tighter control over environmental factors (Pousti et al., 2018). The strong reproducibility in bacterial detection reported in this study suggests that the microfluidic device, including the approach to monitoring biofilm development in real-time and noninvasively using the electrode chemistry technique, is a potentially robust method to shed useful insights on the mechanisms of biofilm development and their eradication.

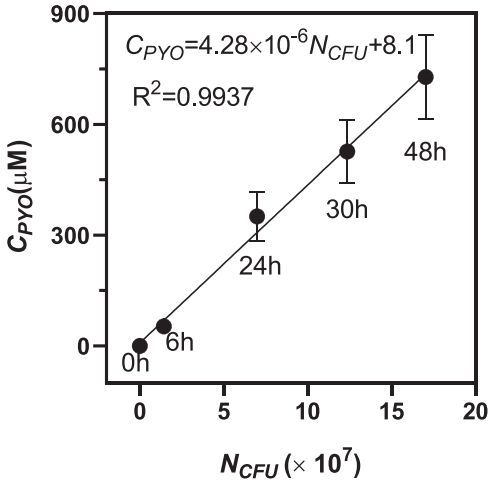

FIGURE 8 Scatter plot of the average value of CFU number (N_{CFU}) of various biofilm ages samples and their corresponding PYO production (C_{PYO}). Error bars represent the standard error of the mean for 36 samples. CFU, colony-forming unit; PYO, pyocyanin.

3.4 | Antibiotic susceptibility

To study the antibiotic susceptibility of ALI biofilm in the microfluidic device, biofilms established in the device after 48 h culture were exposed to CIP solutions of various concentrations (50, 400, 1600 μg/ml), with 400 μg/ml being the MBEC for ALI biofilm, as demonstrated in a previous study (Zhang, Silva, Traini, et al., 2022). To further investigate the biofilm eradication efficacy, the antibiotic susceptibility tests were conducted by applying CIP on the biofilm sample in two different ways of treatment. First, the antibiotic solution was injected into the top chamber, with biofilm submerged in the antibiotic solution. The second option was to inject the antibiotic solution into the bottom chamber, where the antibiotic solution passes through the membrane's pores and diffuses into the biofilm matrix. The top chamber exposure of drugs may infer a drug that has been directly deposited on the surface of the biofilm via pulmonary delivery, while bottom chamber exposure of the drug could loosely infer intravenous or oral administration, with the drug in the systemic circulation, passing through the biological barriers to reach the biofilm site. After 6 h exposure for both treatment ways, the PYO concentration was measured by the electrochemical technique, and the viable cell number was also obtained using the CFU count method. Data was presented using the percentage of the antibiotic-treated sample's value compared with the growth controls' value in the same conditions. Data presented in CFU/ml is provided in the supplementary. It can be observed from the CFU count result (Figure 9a) that CIP induced a concentration-dependent decrease for the biofilm in both drug delivery approaches. When the data were analyzed using one-way ANOVA, which compared the CFU number of antibiotic (C_{CIP} = 50, 400, 1600 μg/ml) treated biofilms with the control group (C_{CIP} = 0 μg/ml), statistically significant differences were observed for 400 μg/ml ($p < 0.01$) and 1600 μg/ml ($p < 0.0001$) CIP solutions. Unpaired *t*-tests were conducted to compare the data between two different drug delivery approaches using the same CIP concentration. The analysis showed that the percentage of viable cell numbers left in biofilm after exposure to the CIP solution via the top chamber was significantly lower ($p < 0.001$) than those contacted with the CIP solution delivered from the bottom chamber of the microfluidic device. The above infers that direct drug deposition on biofilm sites is at least three times more effective than indirect drug exposure. This suggests that considering the biological barrier of epithelial cells and blood vessels, systemic drug delivery (via oral or intravenous administration) is likely challenging and less effective in treating pulmonary infections compared to pulmonary drug delivery, where drugs can be in contact with the infection region when administered directly.

The electrochemical measurement result is displayed in Figure 9b. One-way ANOVA was conducted to compare the PYO concentration of antibiotic (C_{CIP} = 50, 400, 1600 μg/ml) treated biofilms to the control group (C_{CIP} = 0 μg/ml). A statistically significant reduction in PYO production can be observed after being treated with CIP solution using both drug delivery approaches. However, the reduction of *p* value was only found in the top chamber

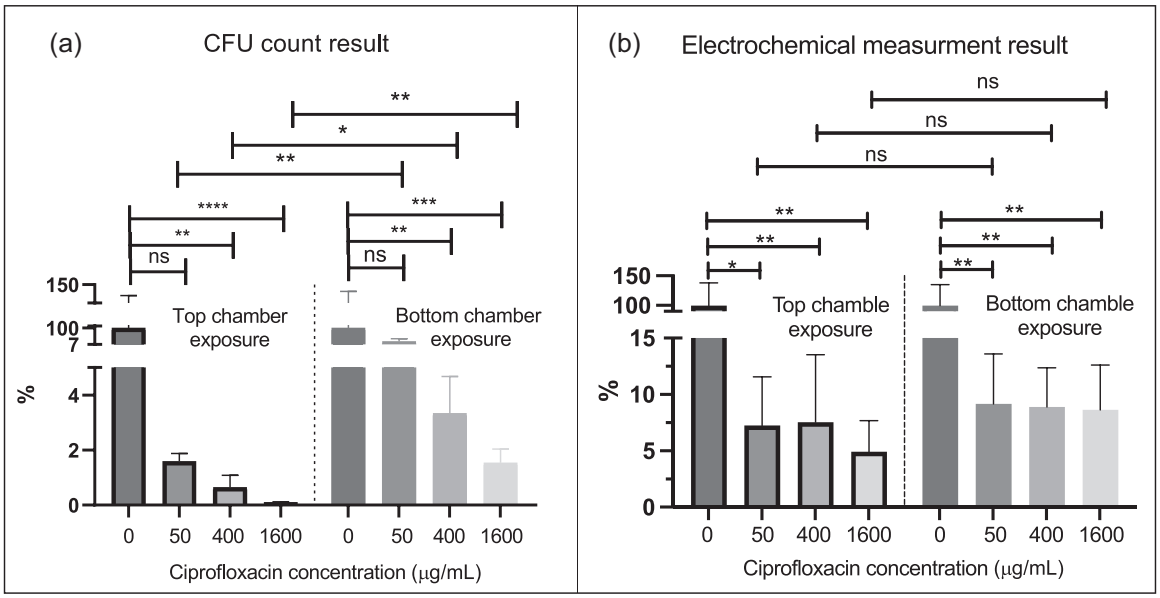

FIGURE 9 Comparison of biofilm killing effect of CIP (50, 400, and 1600 μg/ml) for 6 h exposure on 48 h-old biofilms cultured on ALI. Antibiotic exposure was performed either from the top chamber or the bottom chamber of the microfluidic device. (a) CFU counts; (b) electrochemical measurements of PYO production by the bacterial cells in biofilms at different time points of exposure to CIP. The significant difference is shown for the indicated comparison ($N = 6$, mean ± SEM; $^{*}p < 0.05$; $^{**}p < 0.01$; $^{****}p < 0.0001$; ns, no statistical significance). CFU, colony-forming unit; CIP, ciprofloxacin; PYO, pyocyanin.

exposure between 50 μg/ml and higher concentrations, and no *p* value variance was shown when the CIP concentration increased in the bottom chamber exposure. The unpaired *t*-tests were conducted to compare the data between two different drug delivery approaches; however, unlike the CFU counting results shown in Figure 9a, no statistically significant difference was found. A possible reason for the above is that although a significant number of bacteria has been killed when exposed to the antibiotic solution, there could still be persister cells that exhibit high resistance against antibiotics which may produce PYO at a higher rate. The above has been known to be coordinated by quorum sensing to increase the viability of the community to survive under environmental stresses (Bhargava et al., 2014; Castañeda-Tamez et al., 2018). In addition, it can be observed that, unlike the biofilm growth process, there is no direct correlation between the results obtained from CFU count and PYO electrical measurement upon treating the biofilms with the antibiotic. Therefore, while our established method can be used as an adjuvant to already established methods, it should not be used independently to determine a compound's activity against biofilm bacteria.

Indeed, results from our previous study show that the biofilm cultured using the exact same protocol described in this study is condensed, thick, and has very low permeability. The biofilms demonstrate extremely high resistance to the CIP solution, such that even 1600 μg/ml CIP solution cannot completely eradicate the biofilm. It is well known that bacteria in biofilm are 100–1000 times more tolerant to antimicrobials than corresponding planktonic cells (Hoyle & Costerton, 1991; Olsen, 2015). Also, biofilm-associated cells grow significantly slower than planktonic cells and, as a result, can be slower in taking up antimicrobial agents (Donlan & Costerton, 2002). We also believe that the biofilm's resistance to antibiotics is related to the function of EPS, which present a diffusional barrier that delays the penetration of antimicrobial agent through the biofilm matrix (Donlan & Costerton, 2002; Suci et al., 1994).

4 | LIMITATIONS

Despite the new findings obtained in this study, there are several inherent limitations in the experimental study design that may be considered when interpreting the results. A limitation of the study is that some bacteria may have attached to the WEs during inoculation, which may have affected measurement accuracy. However, considering that the bacteria attached to the electrode has no access to nutrient resources and that the electrode's surface area is relatively small (16% of the membrane surface for ALI biofilm growth), the impact of bacteria growth on the electrode is likely negligible, and unlikely to change the outcome of the observations reported. Second, this study cultured the ALI biofilm on a porous membrane without considering the effects of mucus and mucociliary clearance. During lung infection, biofilm resides within the thick mucus layers on the pulmonary epithelial cells with reduced mucociliary clearance (Loo et al., 2018). Future work to study the above using the dual-chamber device demonstrated in this current study is highly feasible. It would enable the establishment of a *P. aeruginosa* biofilm and human epithelial cells co-culture model to study lung infection in a physiologically realistic environment. Third, the biofilm samples investigated were developed under static conditions. However, biofilms are usually developed in a dynamic flow environment.

For example, biofilms developed in the lung are constantly subjected to airflow, and the shear stress induced by airflow in the lung may vary among different patient groups. Hence, it is worthwhile to investigate the properties of biofilm by including a wider range of flow conditions to study biofilm growth and to help develop a more targeted treatment solution. Fourth, in testing the efficacy of different drug delivery approaches, the current study used an antibiotic in solution, which is nonrealistic, albeit providing the first insights into the complex interaction between CIP and PYO. Aerosolised antibiotics have been normally developed to target respiratory tract infections, future work should further investigate emulating the realistic delivery of aerosolized formulations to the biofilm to evaluate efficacies in treating pulmonary infections by the proposed device. In addition, while this study has validated the PYO measurement using viable cell number count, a more comprehensive and detailed validation on the use of electrode chemistry technique presented in this current work to detect PYO in real-time is warranted. This is, however, beyond the scope of this current work, as this research aims to investigate how PYO changes in real time without disrupting the biofilm. Furthermore, it would be useful to study the biofilm surface adsorption and bacteria's natural deposition longitudinally, but these are difficult to realize without disrupting the biofilm, and doing so would not be in line with the goal of this current work. There is clear merit to develope markers and their relevant electrodes and sensors to monitor these biofilm properties non-invasively in future. Finally, it should be noted that PYO production likely varies depending on the strain of *P. aeruginosa* used. In this study, we tested the PYO production of PAO1, and what applies to PAO1 may not necessarily apply to other strains.

5 | CONCLUSION

A novel dual-chamber microfluidic device intergraded with electrochemical CNFs-modified carbon electrodes was developed. To the best of the authors' knowledge, electrochemical measurement of biofilm grown under the ALI condition is demonstrated for the first time. This state-of-the-art novel device constitutes a physiobiological-relevant biofilm culture model and allows for real-time, noninvasive and *in-situ* electrochemical monitoring of biofilm metabolic activity and treatment efficacy assessment. This current study shows that the production of PYO from bacterial cells in ALI biofilm is correlated to the number of viable cells, with rapid bacteria growth in the first 30 h. Furthermore, comparing CIP treatment using two different drug delivery approaches, loosely mimicking the respiratory and intravenous drug administration, showed that direct exposure to drugs on biofilm is at least three times more effective based on the device setup, design, and membrane properties defined in this current work. Finally, it is important to note that most of the published work on biofilm are in vitro models developed on SLI. The real-time biomarkers measurements presented in this current study which shed light on how biofilm develops under different conditions, are new. Discoveries presented in this study are useful and critical to paving the way to study how ALI biofilms thrive in more complex environmental conditions.

AUTHOR CONTRIBUTIONS

The project was conceptualized by Shaokoon Cheng, Hui Xin Ong, and Ye Zhang. Experiments conduction and data analysis were performed by Ye Zhang with advice and supervision by all co-authors. The manuscript was written by the first author with review and editing from Shaokoon Cheng, Hui Xin Ong, Ye Zhang, Daniela Traini, and Hanieh Gholizadeh.

ACKNOWLEDGMENT

This study was supported by Marie Bashir Institute and Macquarie University Research Excellence Scholarship. Open access publishing facilitated by Macquarie University, as part of the Wiley - Macquarie University agreement via the Council of Australian University Librarians.

CONFLICT OF INTEREST

The authors declare no conflict of interest.

DATA AVAILABILITY STATEMENT

The datasets generated during and/or analyzed during the current study are available from the corresponding author on reasonable request.

ORCID

Ming Li http://orcid.org/0000-0001-7450-6205

REFERENCES

Akiyama, T., Williamson, K. S., & Franklin, M. J. (2018). Expression and regulation of the *Pseudomonas aeruginosa* hibernation promoting factor. *Molecular Microbiology*, *110*(2), 161–175. https://doi.org/10.1111/mmi.14001

Allen, L., Dockrell, D. H., Pattery, T., Lee, D. G., Cornelis, P., Hellewell, P. G., & Whyte, M. K. B. (2005). Pyocyanin production by *Pseudomonas aeruginosa* induces neutrophil apoptosis and impairs neutrophil-mediated host defenses in vivo. *The Journal of Immunology*, *174*(6), 3643–3649. https://doi.org/10.4049/jimmunol.174.6.3643

Amin, R., Knowlton, S., Hart, A., Yenilmez, B., Ghaderinezhad, F., Katebifar, S., Messina, M., Khademhosseini, A., & Tasoglu, S. (2016). 3D-printed microfluidic devices. *Biofabrication*, *8*, 022001.

Azeredo, J., Azevedo, N. F., Briandet, R., Cerca, N., Coenye, T., Costa, A. R., Desvaux, M., Di Bonaventura, G., Hébraud, M., Jaglic, Z., Kačániová, M., Knøchel, S., Lourenço, A., Mergulhão, F., Meyer, R. L., Nychas, G., Simões, M., Tresse, O., & Sternberg, C. (2017). Critical review on biofilm methods. *Critical Reviews in Microbiology*, *43*(3), 313–351. https://doi.org/10.1080/1040841X.2016.1208146

Bai, Z., Dong, W., Ren, Y., Zhang, C., & Chen, Q. (2018). Preparation of Nano Au and Pt alloy microspheres decorated with reduced graphene oxide for nonenzymatic hydrogen peroxide sensing. *Langmuir*, *34*(6), 2235–2244. https://doi.org/10.1021/acs.langmuir.7b02626

Bhargava, N., Sharma, P., & Capalash, N. (2014). Pyocyanin stimulates quorum sensing-mediated tolerance to oxidative stress and increases persister cell populations in *Acinetobacter baumannii*.

Infection and Immunity, *82*(8), 3417–3425. https://doi.org/10.1128/IAI.01600-14

Bjarnsholt, T. (2013). The role of bacterial biofilms in chronic infections. *APMIS*, *121*(136), 1–58. https://doi.org/10.1111/apm.12099

Brazas, M. D., & Hancock, R. E. W. (2005). Ciprofloxacin induction of a susceptibility determinant in *Pseudomonas aeruginosa*. *Antimicrobial Agents and Chemotherapy*, *49*(8), 3222–3227. https://doi.org/10.1128/AAC.49.8.3222-3227.2005

Caldwell, C. C., Chen, Y., Goetzmann, H. S., Hao, Y., Borchers, M. T., Hassett, D. J., Young, L. R., Mavrodi, D., Thomashow, L., & Lau, G. W. (2009). *Pseudomonas aeruginosa* exotoxin pyocyanin causes cystic fibrosis airway pathogenesis. *The American Journal of Pathology*, *175*(6), 2473–2488. https://doi.org/10.2353/ajpath.2009.090166

Castañeda-Tamez, P., Ramírez-Peris, J., Pérez-Velázquez, J., Kuttler, C., Jalalimanesh, A., Saucedo-Mora, M. Á., Jiménez-Cortés, J. G., Maeda, T., González, Y., Tomás, M., Wood, T. K., & García-Contreras, R. (2018). Pyocyanin restricts social cheating in *Pseudomonas aeruginosa*. *Frontiers in Microbiology*, *9*, 9. https://doi.org/10.3389/fmicb.2018.01348

Ceri, H., Olson, M. E., Stremick, C., Read, R. R., Morck, D., & Buret, A. (1999). The calgary biofilm device: New technology for rapid determination of antibiotic susceptibilities of bacterial biofilms. *Journal of Clinical Microbiology*, *37*(6), 1771–1776. https://doi.org/10.1128/JCM.37.6.1771-1776.1999

Donlan, R. M., & Costerton, J. W. (2002). Biofilms: Survival mechanisms of clinically relevant microorganisms. *Clinical Microbiology Reviews*, *15*(2), 167–193. https://doi.org/10.1128/CMR.15.2.167-193.2002

Emanuel, G., & Lorrence, H. G. (2021). *Practical handbook of microbiology*. CRC Press.

Erbay, C. (2016). *Micro/nano technologies for achieving sustainable microbial electrochemical cell systems*. In A. Han, J. Ji, E. Sanchez-Sinencio, & C. Yu (Eds.), ProQuest Dissertations Publishing.

Gholizadeh, H., Ong, H. X., Bradbury, P., Kourmatzis, A., Traini, D., Young, P., Li, M., & Cheng, S. (2021). Real-time quantitative monitoring of in vitro nasal drug delivery by a nasal epithelial mucosa-on-a-chip model. *Expert Opinion on Drug Delivery*, *18*, 803–818. https://doi.org/10.1080/17425247.2021.1873274

Hoyle, B. D., & Costerton, J. W. (1991). Bacterial resistance to antibiotics: The role of biofilms. Progress in drug research. *Fortschritte der Arzneimittelforschung. Progrès des recherches pharmaceutiques*, *37*, 91–105. https://doi.org/10.1007/978-3-0348-7139-6_2

Jamal, M., Ahmad, W., Andleeb, S., Jalil, F., Imran, M., Nawaz, M. A., Hussain, T., Ali, M., Rafiq, M., & Kamil, M. A. (2018). Bacterial biofilm and associated infections. *Journal of the Chinese Medical Association*, *81*(1), 7–11. https://doi.org/10.1016/j.jcma.2017.07.012

Kim, K. P., Kim, Y.-G., Choi, C.-H., Kim, H.-E., Lee, S.-H., Chang, W.-S., & Lee, C.-S. (2010). In situ monitoring of antibiotic susceptibility of bacterial biofilms in a microfluidic device. *Lab On a Chip*, *10*, 3296–3299.

Lau, G. W., Hassett, D. J., Ran, H., & Kong, F. (2004). The role of pyocyanin in *Pseudomonas aeruginosa* infection. *Trends in Molecular Medicine*, *10*(12), 599–606. https://doi.org/10.1016/j.molmed.2004.10.002

Loo, C.-Y., Lee, W. H., Lauretani, G., Scalia, S., Cipolla, D., Traini, D., Young, P., & Ong, H. X. (2018). Sweetening inhaled antibiotic treatment for eradication of chronic respiratory biofilm infection. *Pharmaceutical Research*, *35*, 50.

Maurice, N. M., Bedi, B., & Sadikot, R. T. (2018). *Pseudomonas aeruginosa* biofilms: Host response and clinical implications in lung infections. *American Journal of Respiratory Cell and Molecular Biology*, *58*(4), 428–439. https://doi.org/10.1165/rcmb.2017-0321TR

Miller, M. B., & Bassler, B. L. (2001). Quorum Sensing in Bacteria. *Annual Review Of Microbiology*, *55*(1), 165–199. https://doi.org/10.1146/annurev.micro.55.1.165

Olsen, I. (2015). Biofilm-specific antibiotic tolerance and resistance. *European Journal of Clinical Microbiology & Infectious Diseases: Official publication of the European Society of Clinical Microbiology*, *34*(5), 877–886. https://doi.org/10.1007/s10096-015-2323-z

Park, A., Jeong, H.-H., Lee, J., Kim, K. P., & Lee, C.-S. (2011). Effect of shear stress on the formation of bacterial biofilm in a microfluidic channel. *BioChip Journal*, *5*(3), 236–241. https://doi.org/10.1007/s13206-011-5307-9

Peeters, E., Nelis, H. J., & Coenye, T. (2008). Comparison of multiple methods for quantification of microbial biofilms grown in microtiter plates. *Journal of Microbiological Methods*, *72*(2), 157–165. https://doi.org/10.1016/j.mimet.2007.11.010

Pérez-Rodríguez, S., García-Aznar, J. M., & Gonzalo-Asensio, J. (2022). Microfluidic devices for studying bacterial taxis, drug testing and biofilm formation. *Microbial Biotechnology*, *15*(2), 395–414. https://doi.org/10.1111/1751-7915.13775

Pousti, M., Zarabadi, M. P., Abbaszadeh Amirdehi, M., Paquet-Mercier, F., & Greener, J. (2019). Microfluidic bioanalytical flow cells for biofilm studies: A review. *The Analyst*, *144*(1), 68–86. https://doi.org/10.1039/c8an01526k

Ranganathan, V. (2014). Biofilms: Microbial cities of scientific significance. *Journal of Microbiology & Experimentation*, *1*(3), 00014. https://doi.org/10.15406/jmen.2014.01.00014

Schwartz, K., Stephenson, R., Hernandez, M., Jambang, N., & Boles, B. R. (2010). The use of drip flow and rotating disk reactors for staphylococcus aureus biofilm analysis. *Journal of Visualized Experiments*, (46). https://doi.org/10.3791/2470

Sezgintürk, M. K. (2020). Chapter One—Introduction to commercial biosensors. In M. K. Sezgintürk (Ed.), *Commercial Biosensors and Their Applications* (pp. 1–28). Elsevier.

Shinwari, M. W., Zhitomirsky, D., Deen, I. A., Selvaganapathy, P. R., Deen, M. J., & Landheer, D. (2010). Microfabricated reference electrodes and their biosensing applications. *Sensors*, *10*(3), 1679–1715. Retrieved from https://www.mdpi.com/1424-8220/10/3/1679

Song, J., Li, Y., Yin, F., Zhang, Z., Ke, D., Wang, D., Yuan, Q., & Zhang, X. E. (2020). Enhanced electrochemical impedance spectroscopy analysis of microbial biofilms on an electrochemically in situ generated graphene interface. *ACS Sensors*, *5*, 1795–1803. https://doi.org/10.1021/acssensors.0c00570

Stoodley, P., Dodds, I., Boyle, J. D., & Lappin-Scott, H. M. (1998). Influence of hydrodynamics and nutrients on biofilm structure. *Journal of Applied Microbiology*, *85*(S1), 19S–28S. https://doi.org/10.1111/j.1365-2672.1998.tb05279.x

Subramanian, S., Huiszoon, R. C., Chu, S., Bentley, W. E., & Ghodssi, R. (2020). Microsystems for biofilm characterization and sensing–A review. *Biofilm*, *2*, 100015. https://doi.org/10.1016/j.bioflm.2019.100015

Suci, P. A., Mittelman, M. W., Yu, F. P., & Geesey, G. G. (1994). Investigation of ciprofloxacin penetration into *Pseudomonas aeruginosa* biofilms. *Antimicrobial Agents and Chemotherapy*, *38*(9), 2125–2133. https://doi.org/10.1128/aac.38.9.2125

Webster, T. A., & Goluch, E. D. (2012). Electrochemical detection of pyocyanin in nanochannels with integrated palladium hydride reference electrodes. *Lab on a Chip*, *12*(24), 5195–5201. https://doi.org/10.1039/C2LC40650K

Webster, T. A., Sismaet, H. J., Chan, I. J., & Goluch, E. D. (2015). Electrochemically monitoring the antibiotic susceptibility of *Pseudomonas aeruginosa* biofilms. *The Analyst*, *140*(21), 7195–7201. https://doi.org/10.1039/c5an01358e

Willcox, M. D. P., Zhu, H., Conibear, T. C. R., Hume, E. B. H., Givskov, M., Kjelleberg, S., & Rice, S. A. (2008). Role of quorum sensing by *Pseudomonas aeruginosa* in microbial keratitis and cystic fibrosis. *Microbiology*, *154*(Pt), 2184–2194. https://doi.org/10.1099/mic.0.2008/019281-0

Williams, D. L., & Bloebaum, R. D. (2010). Observing the biofilm matrix of Staphylococcus epidermidis ATCC 35984 grown using the CDC

biofilm reactor. *Microscopy and Microanalysis*, *16*(2), 143–152. https://doi.org/10.1017/S143192760999136X

Zhang, Y., Silva, D. M., Traini, D., Young, P., Cheng, S., & Ong, H. X. (2022). An adaptable microreactor to investigate the influence of interfaces on *Pseudomonas aeruginosa* biofilm growth. *Applied Microbiology and Biotechnology*, *106*, 1067–1077. https://doi.org/10.1007/s00253-021-11746-5

Zhang, Y., Silva, D. M., Young, P., Traini, D., Li, M., Ong, H. X., & Cheng, S. (2022). Understanding the effects of aerodynamic and hydrodynamic shear forces on *Pseudomonas aeruginosa* biofilm growth. *Biotechnology and Bioengineering*, *119*(6), 1483–1497. https://doi.org/10.1002/bit.28077

Žukovskaja, O., Jahn, I., Weber, K., Cialla-May, D., & Popp, J. (2017). Detection of *Pseudomonas aeruginosa* metabolite pyocyanin in water and saliva by employing the SERS technique. *Sensors*, *17*(8), 1704. https://doi.org/10.3390/s17081704

SUPPORTING INFORMATION

Additional supporting information can be found online in the Supporting Information section at the end of this article.

How to cite this article: Zhang, Y., Gholizadeh, H., Young, P., Traini, D., Li, M., Ong, H. X., & Cheng, S. (2023). Real-time in-situ electrochemical monitoring of *Pseudomonas aeruginosa* biofilms grown on air–liquid interface and its antibiotic susceptibility using a novel dual-chamber microfluidic device. *Biotechnology and Bioengineering*, 120, 702–714. https://doi.org/10.1002/bit.28288